Article

Analysis of the Influence of the Gas Infrared Heater and Equipment Element Relative Positions on Industrial Premises Thermal Conditions

Boris Vladimirovich Borisov, Alexander Vitalievich Vyatkin, Geniy Vladimirovich Kuznetsov, Vyacheslav Ivanovich Maksimov *[iD] and Tatiana Aleksandrovna Nagornova [iD]

School of Energy and Power Engineering, National Research Tomsk Polytechnic University, Tomsk 634050, Russia
* Correspondence: elf@tpu.ru

Abstract: The creation of local heated areas in large-sized premises using systems based on gas infrared heaters has recently become the most rational alternative in terms of energy efficiency. However, the lack of information about the thermal characteristics in such areas limits the effective application of these systems. To determine the main thermal parameters characterizing the scheduled thermal conditions in heated local working areas of industrial premises, experimental and mathematical modeling of heat transfer processes in a closed area with the presence of equipment in it was carried out. The experimental area was equipped with a gas infrared heater and a model of the equipment (a horizontally oriented panel). The system of equations of thermal conductivity, radiant heat transfer, as well as energy and Navier–Stokes was solved by the finite element method. A significant influence of the equipment position on the temperature field and the air movement hydrodynamics in the local working area has been established. The equipment presence in the room intensifies the air movement due to thermal convection and, as a result, a more uniform temperature distribution over the local working area was obtained. Analysis of the obtained results shows the possibility to control the temperature fields' formation in local working areas during the gas infrared heater operation by varying the position and configuration of the equipment in the room.

Keywords: gas infrared heater; heat supply object; local working area; thermal conditions; convective heat transfer

1. Introduction

The analysis of the air thermal state (thermal comfort) in premises (often of average temperature) is relevant in the last decade within the solutions sought for urgent energy conservation problems for many countries [1–6]. To assess this indicator ("comfortable" air temperature), various standards have been developed, for example, ASHRAE 55 [7] and ISO 7730 [8]. However, the average air temperature in the premises cannot be used as the only "comfort" criterion. Accordingly, in many cases the criterion is inappropriate [9,10]. It is necessary to take into account the inhomogeneity of the environment characteristics in the case of any size of premises [10,11] (rather large temperature differences are possible in all coordinate directions). Therefore, balanced calculation methods are not always applicable [12,13]. Forming scheduled thermal conditions [10,14–18] (comfortable air temperature in a local working area) in large-sized industrial premises with a low area load is a particularly difficult task. Since maintaining comfortable indoor conditions in unfavorable weather conditions (low ambient temperatures) requires large energy costs, the thermal conditions problem becomes multifactorial regarding economic, environmental, and publicly significant criteria.

Industrial premises using a standard heating system with hot-water calorifiers [19–25], whose operation is based on the convective heat transfer mechanism, consume a fairly large amount of energy [26–29]. This lead to significant CO_2 emissions [30,31] and high

economic costs [32], since it takes a long time to warm up the air of the entire premises. In addition, most of the thermal energy accumulates in the enclosing structures and in the air closer to the ceiling [33,34]. As a result, in a large premises (8–10 m in height) the staff feel uncomfortable. Too high or too low temperatures on the premises affect the workers overall well-being and their productivity [9,10].

Recently, a lot of research devoted to the heating systems' improvement in terms of large-sized premises has been carried out [17,22,35,36]. The use of convective systems (forcing warm air from the floor distribution system) may not be safe for many industries due to the high dust content. Therefore, the use of gas infrared heaters (GIH) is more appropriate in this case [37–43]. It is known [39,44] that it is easier to provide thermal conditions in a radiant heating system compared to a mechanical ventilation and air conditioning system. However, research into GIH use that concerns energy efficiency is being carried out by only a few authors. Only the average premises temperature and energy savings are the matters that are mostly evaluated [43].

There is an approach in the literature, which proposes to additionally use waste heat recovery (WHR) of flue gas from radiant heaters and evaluated the economic effect of such an engineering solution [45,46]. However, there is still no general theory relating to the operation of gas infrared heaters. Such specific practical issues as the choice of the GIH location according to the premises' dimensions, the power and operating time, the height of the GIH suspension relative to the floor and the worker need to be discussed.

At the same time, there are grounds for the hypothesis that the location of any equipment should influence the temperature in the local working area. The heat from the GIH contributes to open equipment surfaces' heating, and, as a result, circulating flows of air heated from these surfaces are formed [47]. Natural circulation (free convection) of air masses can significantly affect the temperature fields [34,48]. However, it is not always possible to experimentally analyze the influence of this factor.

There are a few publications with the results of theoretical and experimental researches devoted to the radiant heating sources' operation, which can be used for practical and meaningful assessments [34,44]. The lack of information about the thermal conditions of working areas with GIH operating, the proportion of rationally used heat generated, surface temperatures (located at different heights under the GIH or in its vicinity) limits the effectiveness of development work to design radiant heating systems for local working areas of industrial premises. Moreover, it is necessary to consider the indoor equipment effects.

The aim of the work was to analyze the influence of equipment located in the local working area of large premises with an infrared heating system on the thermal conditions of such an area based on the experimental and theoretical results.

2. Experimental Investigations

2.1. Selecting Data for the Experiments

The data selection for the development of a method for conducting experimental studies of heating large-sized premises with a gas infrared heater was made based on previous studies [33,44,49,50] and other online sources.

It was established that the distribution of heat fluxes and temperatures over large areas under the several (three to four) operating gas infrared heaters are equidistant in areas heated by one heater [49,50]. Additionally, the dependences of the heat fluxes density entering the working area from heaters with a different power (from 5 to 30 kW) in the zone between the radiation source and the heating surface were determined experimentally [33,49]. A conclusion was drawn about the applicability of a low-power GIH for heating a local area in which working, servicing equipment is located [33,44,49,50]. One medium-power (5 kW) gas infrared heater located at a height of 3 m from the floor surface of the experimental area was used during the experiments.

Experimental studies were carried out in the winter season, when the outdoor air temperature T_e varied from $-12\ °C$ to $-30\ °C$ (typical experimental results at $T_e = -22\ °C$ are presented below). The initial temperature of the air inside the experimental area was in

a range from +2 °C to +15 °C. Such a temperature range is fairly representative for two-shift or one-shift operation premises. However, reduction in the indoor air temperature to negative values in the overwhelming majority of the variants is inappropriate for objective reasons. For this reason, the experiments were mainly carried out at an indoor temperature of +10 °C. It needs to be mentioned that the quality of air inside the industrial premises is regulated by the norms and rules of industrial sanitation. The air should not contain any dust particles and its humidity value needs to fall within the range from 15% to 75% [7,9]. Such an air state was ensured during the experiments.

2.2. Experimental Box and Equipment

Setup presented on Figure 1 was used to conduct the research. The main elements of the setup were: a light type gas infrared heater—GIH-5 (produced by Sibshvank, Tyumen, Russia) with a nominal thermal power Q_{V_GIH} = 5 kW and a radiant efficiency η_{Rad} = 0.57; a gas source; a model of the heat supply object; Chromel-Alumel-type thermocouples with an insulating PFA fluoropolymer coating (junction thickness 0.08 mm); an analog-to-digital converter (National Instruments network converter with a DAQ 9181) allowing for control of the clocking, synchronization and data transmission from a 16-channel 32-bit isothermal temperature measurement module NI 9214 (National Instruments, Austin, TX, USA); a workstation for the data storage and analysis (personal computer).
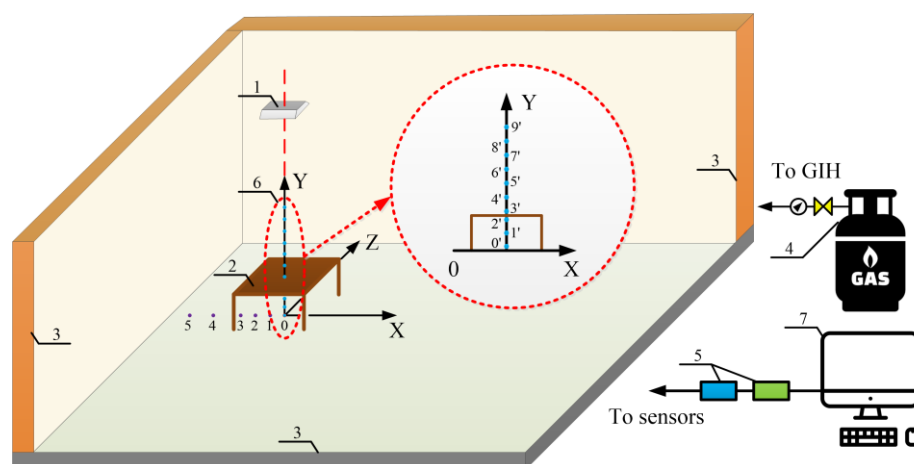

Figure 1. Scheme of the experimental area and thermocouple location: 1—GIH; 2—remote horizontal panel; 3—enclosing structures; 4—shut-off and control valves of the gas supply system; 5—analog-to-digital converter (NI 9214) and data collection and transmission system (DAQ 9181); 6—thermocouples (0′–9′ thermocouple numbers); 7—computer.

Modeling of heat transfer processes was carried out for a typical premises corresponding to a real heat-supply object, heated by a gas infrared heater. The premises used for carrying out the experiments was closed, with dimensions of 5 × 4.4 × 11 m (Figure 1). The premises has brick walls 0.700 m thick, and floor and ceiling from reinforced concrete slab 0.25 m thick. There is a 0.3 m unheated air gap between the ground and the floor. A 0.1 m mineral wool layer was used for the ceiling slab insulation. There is an attic space with a height of 1.5 m. The roof is gabled with a supporting frame of 0.2 m wooden beam. The roof is coated with 0.03 m galvanized steel. The distance between the center of the GIH projection and the left wall was 1.6 m. The lower heater surface was placed at the 3 m distance from the floor. In the premises, there was an experimental frame made of aluminum pipes 0.015 m in diameter with a plastic outer coating, which made it possible to place a horizontal panel at different heights from the floor. The panel (Figure 2) has a width of 1.2 m and a thickness of 0.04 m. The panel is made of wood material (Table 1). The highly thermally conductive material and the small diameter of the tubes make it possible to assume that the frame used does not significantly affect the thermal conditions in the premises.
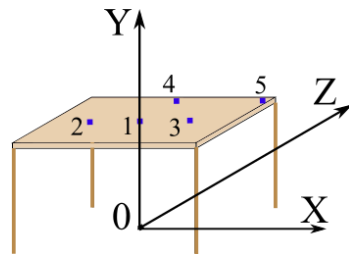
Figure 2. Thermocouples' arrangement on the panel: 1—point under the GIH; 2—point at a distance of 0.3 m from the GIH center in the longitudinal direction; 3—point on the edge of the table in the longitudinal direction from the GIH center (0.6 m); 4—a point on the edge of the table in the transverse direction from the center of the GIH (0.28 m); 5—a point in the corner of the panel.

Table 1. Thermophysical properties of the materials (enclosing structures and panel) used in the experiments [51,52].

Object	Thickness (m)	Material	Density (kg m^{-3})	Heat Capacity (J kg^{-1} K^{-1})	Thermal Conductivity (W K^{-1} m^{-1})	Blackness
Floor, ceiling, walls	0.1	Concrete	2500	2400	1.55	0.95
Walls	0.7	Brick	1700	880	0.81	0.93
Horizontal panel	0.02	Pine	520	2300	0.15	0.4

Temperatures and heat-flux densities were measured on the enclosing structures and the horizontal panel surfaces (Figure 2) in real-time mode. Additionally, air temperatures were recorded at various points in the zone of GIH influence (Figure 1 and Table 2).

Table 2. Coordinates of the thermocouples' location (Figures 1 and 2) in the measurement area.

Air Temperature Measurement										
Thermocouple Numbers	0′	1′	2′	3′	4′	5′	6′	7′	8′	9′
X, m	0	0	0	0	0	0	0	0	0	0
Z, m	0	0	0	0	0	0	0	0	0	0
Y, m	0.05	0.4	0.74	0.755	1.0	1.2	1.4	1.6	1.8	2.0
Floor temperature measurement										
Thermocouple numbers	0	1		2		3		4		5
X, m	0	−0.2		−0.4		−0.6		−0.8		−1
Z, m	0	0		0		0		0		0
Y, m	0	0		0		0		0		0
Temperature measurement on the panel in the GIH influence zone										
	1 s		2 s		3 s		4 s		5 s	
X, m	0		−0.3		0.3		0		0.6	
Z, m	0		0		0		0.28		0.28	
Y, m	0.755		0.755		0.755		0.755		0.755	

In addition, to substantiate the conclusions about the conditions for creating regulated thermal regimes during the GIH operation, an analysis was completed of the air temperature distributions in the vertical section ($0 \leq Y \leq 2.0$ m), at a distance of 0.2 m to the left ($X = 0.8$ m) and to the right ($X = 2.4$ m) from panels (Figure 1). It is assumed that there should be a worker in this zone.

2.3. Experimental Technique

The Chromel-Alumel (80 μm junction diameter) thermocouples were used to carry out the measurements. The measurement error was no more than 0.4 °C. The quality of thermal contact between the thermocouples and the object surface was ensured by using KPT-8

thermal paste. Such an approach also provides protection against re-radiation. The analog-to-digital converter and the data acquisition system were located at a distance of 4 m from the measurement surface on a heat-insulated lining with protection against re-radiation for testing by thermostat the cold junction built into them.

A special measuring complex, consisting of an analog-to-digital converter (NI 9214) and input/output module (NI with DAQ 9171) was used to record thermocouple signals. The time interval was less than 2 s.

The obtained data processing was carried out by a personal computer. Typical examples of temperature distribution in time at twelve points of the analysis area (oscillograms) are shown in Figures 3–5. The number of experiments for each case was at least three to eliminate measurement errors. The values of the standard deviations and the corresponding variation coefficients did not exceed 4%. Statistical processing of the results was necessary to consider the possibility of influencing of minor deviations from the normalized numerical values of the factors of the second and third significance levels (pressure, air humidity, ambient temperature changes during long-term experiments). The scale of such influence was insignificant. However, according to the theory of errors in experimental studies, it is still necessary to take into account such factors when assessing the reliability of the measurement results.

(a)

(b)
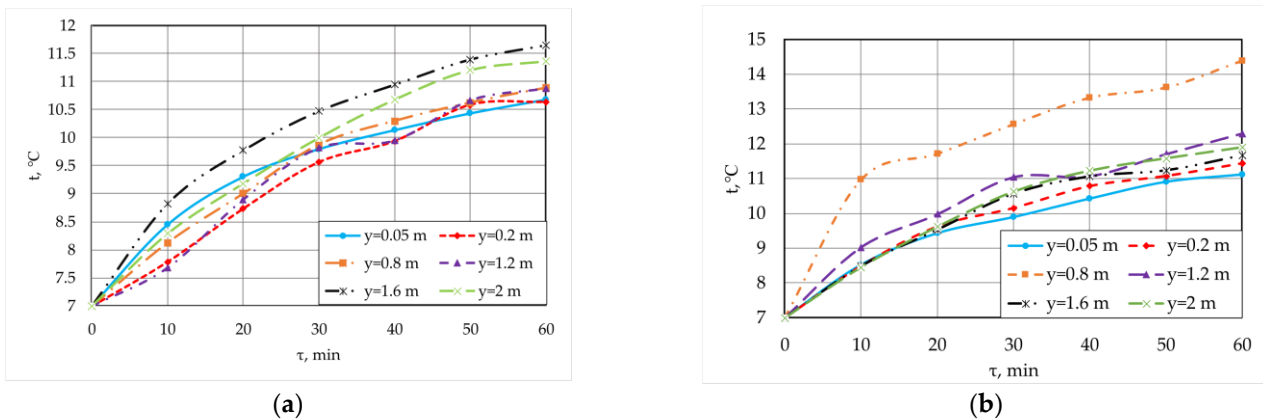
Figure 3. Air temperatures change with increasing time at the points of thermocouples' location on the GIH symmetry axis: (**a**) premises without equipment; (**b**) the panel is located at a height of 0.755 m from the floor.
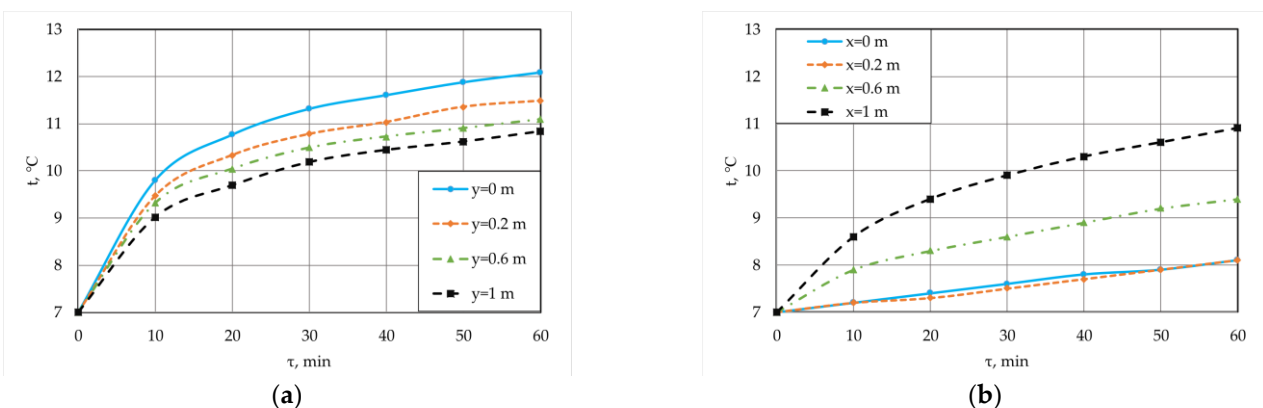

(a)

(b)

Figure 4. Floor surface temperatures change with increasing time at $0 \le X \le 1.0$ m, $Y = 0$: (**a**) premises without equipment; (**b**) the panel is located at a height of 0.755 m from the floor.
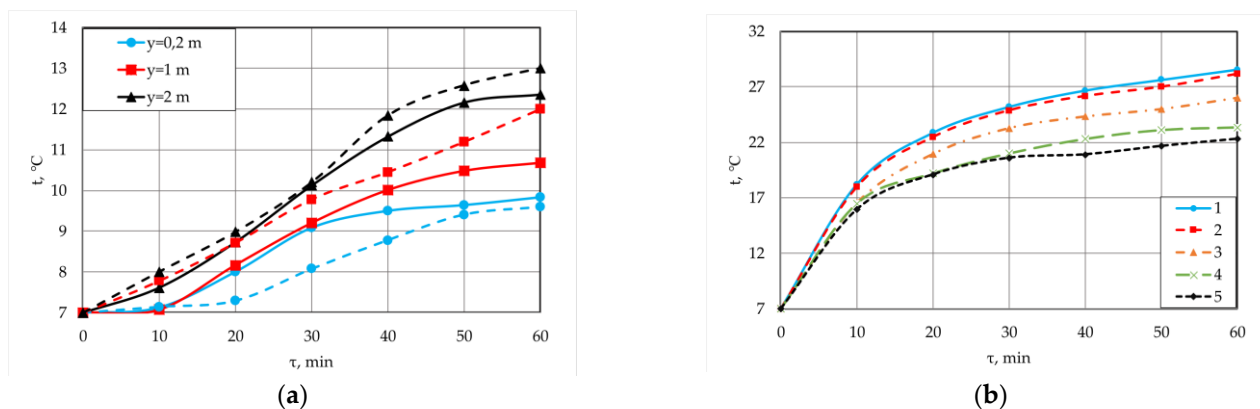
(a)　　　　　　　　　　　　　　　　　　　　　　　　　　　**(b)**

Figure 5. Air temperatures change (**a**) with increasing time on the left X = 0.8 m (solid line) and on the right X = 2.4 m (dashed line) from the panel at points at a distance of 0.2 m; 1.0 m; 2.0 m from the floor and changes in panel surface temperatures; (**b**) (1–5 thermocouples location in accordance with Table 2 and Figure 2).

2.4. The Main Experimental Results

Typical results of temperature measurements at characteristic points and sections are shown in Figures 3–5. Experiments were conducted in a large premises free of equipment with a working gas infrared heater first. Then, a horizontal panel that simulates the equipment was added to the premises. Experiments have shown that for 50 min of GIH operation, the surface temperature increases most intensively. Further, temperature changes by less than 1 degree. Therefore, the figures show the experimental results in the range of time changes up to 60 min. Based on the obtained temperature distributions analysis (Figures 3 and 4), regularities of the complex (radiative-conductive-convective) heat transfer processes can be defined.

The air temperature at each point of the premises without a panel (Figure 3a) increases with an increase in time and at τ = 60 min reaches 11.3 °C at a height slightly higher than human height (Y = 2.0 m is the approximate upper boundary of the local working area). The panel in the zone of direct GIH exposure (Figure 3b) affects the heating of air masses located above it.

The floor surface temperatures in the central part of the GIH influence zone (Figure 4b) after 20 min of its operation change insignificantly, but with distance from the GIH symmetry axis, the temperature values decrease.

To substantiate the conclusions about creating scheduled thermal conditions during the GIH operation, an analysis of the air temperature distributions in the vertical section ($0 \leq Y \leq 2.0$ m) was carried out at a distance of 0.2 m to the left (X = 0.8 m) and to the right (X = 2.4 m) from the panel (Figure 5). It is assumed that a worker should be located in this area.

It was previously established [50] that the worker temperature regime in the infrared heating zone is influenced not only by the basic heater characteristics, but also by the air temperature near the clothing surface. The smaller the difference in air temperature along the height, the more comfortable the worker will feel [53].

The results in Figure 5 illustrate some inhomogeneities of the temperature field at a distance of 0.2 m to the left and right of the panel. The difference t in height (from 0.2 to 2 m) is 3.4 °C. It should also be noted that the panel surface temperatures (Figure 5b) are significantly higher than the concrete floor surface temperatures (Figure 4b) at all thermocouples' locations. Most likely, it is due to the differences in the thermal conductivity values of concrete and wood. Accordingly, the concrete floor heats up to a great depth and its surface temperature is significantly lower than a wood panel.

3. Mathematical Statement and Solution Method

Numeric simulation was carried out in the framework of a two-dimensional approximation. We considered a rectangular area with dimensions $L_x = 5 \times L_y = 4.4$ m, bounded by the floor, walls and ceiling (enclosing structures, Table 1) with a wall thickness of $L_{wall} = 0.1$ m (Figure 5) with two horizontal structural elements (Figure 6) corresponding to the GIH (dimensions $Lx_{GIH} = 0.4$ m, $Ly_{GIH} = 0.05$ m) and panel (dimensions $Lx_{tb} = 1.2$ m, $Ly_{tb} = 0.04$ m).
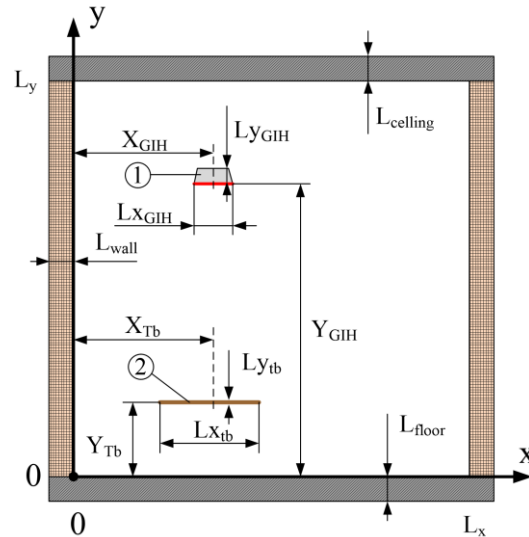

Figure 6. Problem solution area: 1—GIH; 2—Panel.

The location coordinates of the radiant energy source and the horizontal panel corresponded to the most typical variation in their placement in a real premises (Figure 1). Coordinates (X_{Tb}, Y_{Tb}) of the upper boundary center of the horizontal remote panel surface varied in the x and y directions. The value of air pressure was taken as $p_{air} = 0.1$ MPa and did not change with time in the entire problem solution area. When modeling radiative heat transfer, air was considered a diathermic medium, and all surfaces (enclosing structures, GIH and equipment) were opaque gray.

Convective–conductive heat transfer according to such a physical model was described by the energy equation [54]:

$$\rho c_p \frac{\partial T}{\partial \tau} + \rho c_p \left(\vec{u} \cdot \nabla \right) T = \nabla \cdot (\kappa \nabla T), \tag{1}$$

$-L_{wall} \leq x \leq L_x + L_{wall}, \; -L_{floor} \leq y \leq L_y + L_{ceiling},$
$(x, y) \notin (X_{GIH} - Lx_{GIH}/2 \leq x \leq X_{GIH} + Lx_{GIH}/2, \; Y_{GIH} \leq y \leq Y_{GIH} + Ly_{GIH}),$

where τ, ρ, T, c_p, κ—time, density, temperature, specific isobaric heat capacity and thermal conductivity, respectively.

Velocity vector field $\vec{u}$ was determined from the solution of the system of incompressible gas motion and continuity equations in the Boussinesq approximation [55]:

$$\rho \frac{\partial \vec{u}}{\partial \tau} + \rho \left(\vec{u} \cdot \nabla \right) \vec{u} = \nabla \cdot \left[-p \vec{I} + \vec{K} \right] + (\rho - \rho_0) \vec{g}, \tag{2}$$

$$\frac{\partial \rho}{\partial \tau} + \nabla \cdot \left(\rho \vec{u} \right) = 0, \tag{3}$$

$$0 \leq x \leq L_x, \; 0 \leq y \leq L_y,$$

$(x, y) \notin (X_{GIH} - Lx_{GIH}/2 \leq x \leq X_{GIH} + Lx_{GIH}/2, \; Y_{GIH} \leq y \leq Y_{GIH} + Ly_{GIH}),$
$(x, y) \notin (X_{Tb} - Lx_{Tb}/2 \leq x \leq X_{Tb} + Lx_{Tb}/2, \; Y_{Tb} - Ly_{Tb} \leq y \leq Y_{Tb}),$

where p, $\vec{I}$—pressure and unit tensor symbol; ρ_0, $\vec{g}$—initial density and gravitational acceleration; $\vec{K} = (\mu + \mu_T)\left(\nabla \cdot \vec{u} + \left(\nabla \cdot \vec{u}\right)^T\right) - \frac{2}{3}(\mu + \mu_T)(\nabla \cdot \vec{u})\vec{I} - \frac{2}{3}\rho k \vec{I}$—tensor of viscous friction stresses taking into account the turbulent (index "*T*") component, μ—dynamic viscosity coefficient.

When modeling a turbulent air flow, a "*k-ε*" model was used. In this case, the turbulence dissipation rate (ε) and the kinetic energy of turbulence (k) were determined by the equations [56,57]:

$$\rho\frac{\partial k}{\partial \tau} + \rho\left(\vec{u} \cdot \nabla\right)k = \nabla \cdot \left[\left(\mu + \frac{\mu_T}{\sigma_k}\right)(\nabla \cdot k)\right] + P_k - \rho\varepsilon, \tag{4}$$

$$\rho\frac{\partial \varepsilon}{\partial \tau} + \rho\left(\vec{u} \cdot \nabla\right)\varepsilon = \nabla \cdot \left[\left(\mu + \frac{\mu_T}{\sigma_\varepsilon}\right)(\nabla \cdot k)\varepsilon\right] + C_{\varepsilon 1}\frac{\varepsilon}{k}P_k + C_{\varepsilon 2}\rho\frac{\varepsilon^2}{k}. \tag{5}$$

$$0 \leq x \leq L_x,\ 0 \leq y \leq L_y,$$

$(x,y) \notin (X_{GIH} - Lx_{GIH}/2 \leq x \leq X_{GIH} + Lx_{GIH}/2,\ Y_{GIH} \leq y \leq Y_{GIH} + Ly_{GIH})$,
$(x,y) \notin (X_{Tb} - Lx_{Tb}/2 \leq x \leq X_{Tb} + Lx_{Tb}/2,\ Y_{Tb} - Ly_{Tb} \leq y \leq Y_{Tb})$,

Solutions of Equations (4) and (5) were used to calculate $\mu_T = \rho C_\mu k^2/\varepsilon$. In Equations (4) and (5), the operator has the form $P_k = \mu_T\left[\nabla \cdot \vec{u} : \left(\nabla \cdot \vec{u} + \left(\nabla \cdot \vec{u}\right)^T\right) - \frac{2}{3}\left(\nabla \cdot \vec{u}\right)^2\right] - \frac{2}{3}\rho k\nabla \cdot \vec{u}$. The values of the constants are taken according to the general theory [56]: $C_{\varepsilon 1} = 1.44$, $C_{\varepsilon 2} = 1.92$, $C_\mu = 0.09$, $\sigma_k = 1$, $\sigma_\varepsilon = 1.3$.

Radiation fluxes were calculated using the zonal model [58] with direct integration of fluxes between all components ("Surface-to-Surface Radiation") of a closed system of surfaces at angular coefficients determined within this system.

Temperature values T_0 and zero values of the air-movement velocity components over the entire region were set as the initial conditions.

$$T(0, x, y) = T_0,\ \vec{u}(0, x, y) = 0,\ -L_{wall} \leq x \leq L_x + L_{wall},\ -L_{floor} \leq y \leq L_y + L_{ceiling}.$$

The emitting surface temperature was set constant for the lower GIH surface the entire time of its operation:

$$T(\tau, x, y) = T_{GIH},\ \tau \geq 0,\ X_{GIH} - Lx_{GIH}/2 \leq x \leq X_{GIH} + Lx_{GIH}/2,\ y = Y_{GIH}$$

The adiabaticity conditions on the outer surfaces of the solution area were used as the boundary conditions for Equation (1). This is due to a limited GIH operating time, so the enclosing structures of the premises do not warm up over the entire thickness:

$\nabla T(\tau, x, y) = 0$, at $\tau > 0$,
$(x,y) \in \left(x = -L_{wall}, -L_{floor} \leq y \leq L_y + L_{ceiling}\right) \cup \left(x = -L_{wall}, -L_{floor} \leq y \leq L_y + L_{ceiling}\right) \cup$
$\left(-L_{wall} \leq x \leq L_x + L_{wall}, y = -L_{floor}\right) \cup \left(-L_{wall} \leq x \leq L_x + L_{wall}, y = L_y + L_{ceiling}\right)$.

On the side surfaces of the GIH:

$T(\tau, x, y) = T_{FGIH}$, at $\tau > 0$,
$(x,y) \in (x = X_{GIH} - Lx_{GIH}/2,\ Y_{GIH} \leq y \leq Y_{GIH} + Ly_{GIH}) \cup$
$(x = X_{GIH} + Lx_{GIH}/2,\ Y_{GIH} \leq y \leq Y_{GIH} + Ly_{GIH})$.

T_{F_GIH}—GIH side surfaces' temperature. The results of experimental studies show that the value of T_{F_GIE} practically does not depend on the experimental conditions and is set equal $T_{F\_GIH} = 47 \pm 4\ °C$ to 20 min of GIH operation. Numerical studies show that the value changes of side surfaces' temperature within the given limits practically do not change the temperatures and velocities fields.

On the upper surface of the GIH:

$$\nabla T(\overrightarrow{\tau, x, y}) = -\frac{q_{FGIH}}{\lambda}, \text{ at } \tau > 0,$$
$$(x, y) \in (X_{GIH} - Lx_{GIH}/2 \leq x \leq x = X_{GIH} + Lx_{GIH}/2, \; y = Y_{GIH} + Ly_{GIH}).$$

q_{F_GIH}—the density of the convective heat flux of combustion products. q_{F_GIE} determined by rated heat output (Q_{V_GIH}, B_T), radiant efficiency (η_{Rad}), and the GIH upper surface area (F_{Up_GIH}, m^2) according to the ratio: $q_{F\_GIH} = (1 - \eta_{Rad}) Q_{V\_GIH}/F_{Up\_GIH}$.

The heat flux density to the surface (q_{sol}) is the sum of the conductive–convective heat flux density to this surface (q_{gas}) and the radiation heat density from all radiating surfaces (q_{rad}):

$$q_{sol} = q_{gas} + q_{rad}, \; \tau \geq 0, \; (x, y) \in (x = 0, \; 0 \leq y \leq L_y) \cup (x = L_x, \; 0 \leq y \leq L_y) \cup$$
$$(0 \leq x \leq L_x, \; y = 0) \cup (0 \leq x \leq L_x, \; y = L_y) \cup$$
$$(x = X_{Tb} - Lx_{Tb}/2, \; Y_{Tb} - Ly_{Tb} \leq y \leq Y_{Tb}) \cup (x = X_{Tb} + Lx_{Tb}/2, \; Y_{Tb} - Ly_{Tb} \leq y \leq Y_{Tb}) \cup$$
$$(X_{Tb} - Lx_{Tb}/2 \leq x \leq X_{Tb} + Lx_{Tb}/2, \; y = Y_{Tb} - Ly_{Tb}) \cup$$
$$(X_{Tb} - Lx_{Tb}/2 \leq x \leq X_{Tb} + Lx_{Tb}/2, \; y = Y_{Tb}).$$

The no-slip conditions were set as boundary conditions at the interfaces "gas–solid surface" for the system of Equations (2) and (3) [55,56].

$$\overrightarrow{u}(\tau, x, y) = 0, \; \tau \geq 0, \; (x, y) \in (x = 0, \; 0 \leq y \leq L_y) \cup (x = L_x, \; 0 \leq y \leq L_y) \cup$$
$$(0 \leq x \leq L_x, \; y = 0) \cup (0 \leq x \leq L_x, \; y = L_y) \cup$$
$$(x = X_{Tb} - Lx_{Tb}/2, \; Y_{Tb} - Ly_{Tb} \leq y \leq Y_{Tb}) \cup (x = X_{Tb} + Lx_{Tb}/2, \; Y_{Tb} - Ly_{Tb} \leq y \leq Y_{Tb}) \cup$$
$$(X_{Tb} - Lx_{Tb}/2 \leq x \leq X_{Tb} + Lx_{Tb}/2, \; y = Y_{Tb} - Ly_{Tb}) \cup$$
$$(X_{Tb} - Lx_{Tb}/2 \leq x \leq X_{Tb} + Lx_{Tb}/2, \; y = Y_{Tb}) \cup$$
$$(x = X_{GIH} - Lx_{GIH}/2, \; Y_{GIH} \leq y \leq Y_{GIH} + Ly_{GIH}) \cup$$
$$(x = X_{GIH} + Lx_{GIH}/2, \; Y_{GIH} \leq y \leq Y_{GIH} + Ly_{GIH}) \cup$$
$$(X_{GIH} - Lx_{GIH}/2 \leq x \leq x = X_{GIH} + Lx_{GIH}/2, \; y = Y_{GIH} + Ly_{GIH}) \cup$$
$$(X_{GIH} - Lx_{GIH}/2 \leq x \leq X_{GIH} + Lx_{GIH}/2, \; y = Y_{GIH}).$$

The method of near-wall functions was used near solid surfaces, where viscous effects prevailed over turbulent ones [56].

The system of Equations (1)–(5) with all the initial and boundary conditions was solved with the finite element method using "The Heat Transfer in Fluids' Interface" and "The Turbulent Flow, k-ε Interface" modules of the COMSOL Multiphysics software package. The Surface-to-Surface Radiation module was used to determine the radiation heat flux parameters.

4. Model Verification

Figure 7 shows the temperature and velocities fields calculated as a result of solving the problem formulated above for a premises without equipment. The results are given for the area heated by a gas infrared heater after reaching stationary values of the main process characteristics.

Vortex structures are clearly visible in Figure 7b. They are formed as a result of the radiation flux supply to the floor surface and the air heating directly from the GIH.

Figure 8 shows the temperature and velocity fields when the panel is positioned at a height of Y_{Tb} = 0.755 m centered on the projection of the GIH symmetry axis.
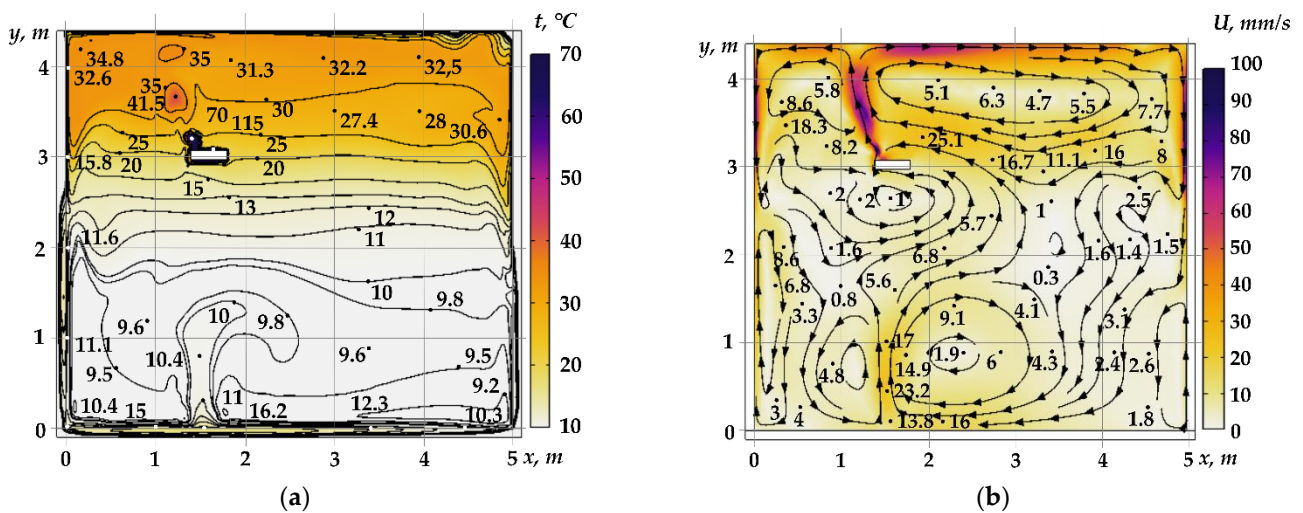
Figure 7. (a) Temperature fields (positions of characteristic isotherms) and (b) streamlines for an area without a panel after τ = 60 min of GIH operation.
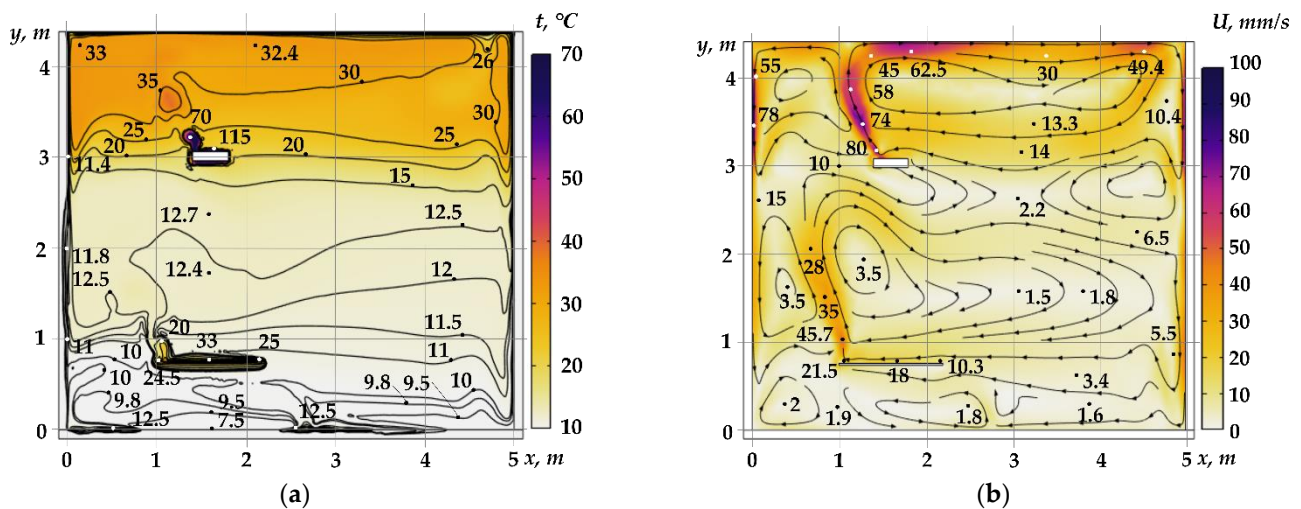
Figure 8. Temperature fields (a) and streamlines (b) for the area with the panel (X_{Tb} = 1.6 m, Y_{Tb} = 0.755 m) in the GIH operation zone (τ = 60 min).

A comparison of Figures 7 and 8 allows the conclusion to be drawn that heating of the air near the panel simulating the equipment can change the flow structure and, accordingly, change the temperature conditions in the considered area. The horizontal panel presence leads to a 2 °C temperature decrease in the lower (*Y* from 0 to 0.755 m) and a 4 °C increase in the upper (*Y* from 0.755 m to 2.0 m) areas of the local working area. These temperature changes occur because the heat dissipation into the panel is much less than under the same floor heating conditions (the thermal conductivity coefficient of the concrete floor is five times higher than such a value for any plastic or wood). Heat dissipation into the panel is much less than under the same floor heating conditions. This is due to the five times difference in thermal conductivity values for the concrete floor and for any plastic or wood material. The horizontal panel acts as a screen that prevents the spread of heat (Figure 8) and at the same time heats up to a temperature of about 36 °C. In this case a sufficiently high air temperature difference occurs in the local zone along the height of the considered area. A zone of air heated to 25 °C is formed above the panel, which rises quite intensively (at a velocity of 35–45 mm/s). The area under the panel practically does not heat up, because thermal radiation from the GIH does not fall on the floor surface. So, the temperature in this zone rises due to the influx of heated masses from adjacent areas (right and left) because of formed low-intensity circulation currents. Thus, if we consider

the temperature conditions of the local areas in which the worker can be located (the area above the panel and the zone 20 cm long to the left and right of it with a height of 0 to 2 m), then the upper part of the worker's body (head, face, neck, chest) will be washed by a stream of heated air from 18 to 25 °C at a velocity of about 35 mm/s.

Figure 9 shows the experimental and theoretical temperature distributions along the height of the premises with and without a panel on the GIH symmetry axis.

(**a**)   (**b**)

Figure 9. Distribution of experimental and theoretical values of air temperatures along the Y coordinate on the GIH symmetry axis (τ = 60 min): (**a**) premises without the panel, and (**b**) with a 0.755 m high panel.

The temperature distributions to the left and to the right of the panel at the same distance of 0.2 m ($X = (X_{Tb} - Lx_{Tb}/2) \pm 0.2$ m), obtained as a result of experimental and numerical studies, are shown in Figure 9. It can be noted that the data have good correspondence along the Y coordinate. At a height of Y = 1.2–1.6 m, a slight increase in temperature values is noticeable both in numerical studies and in the experiments (Figure 10). This is due to the formation of a large-scale circulation vortex in the area under study. The temperature change along with the height to the left of the panel is more pronounced (Figure 10a). This phenomenon is related to the fact that the flow of air heated from the panel, rising upwards, deviates to the left and turns out to be in the section X = 0.8 m at a height Y = 1.2–1.6 m from the floor (Figure 8b). The temperature increase to the right of the panel at the same height (Figure 10b) is also caused by the vortex circulation flow.

(**a**)   (**b**)

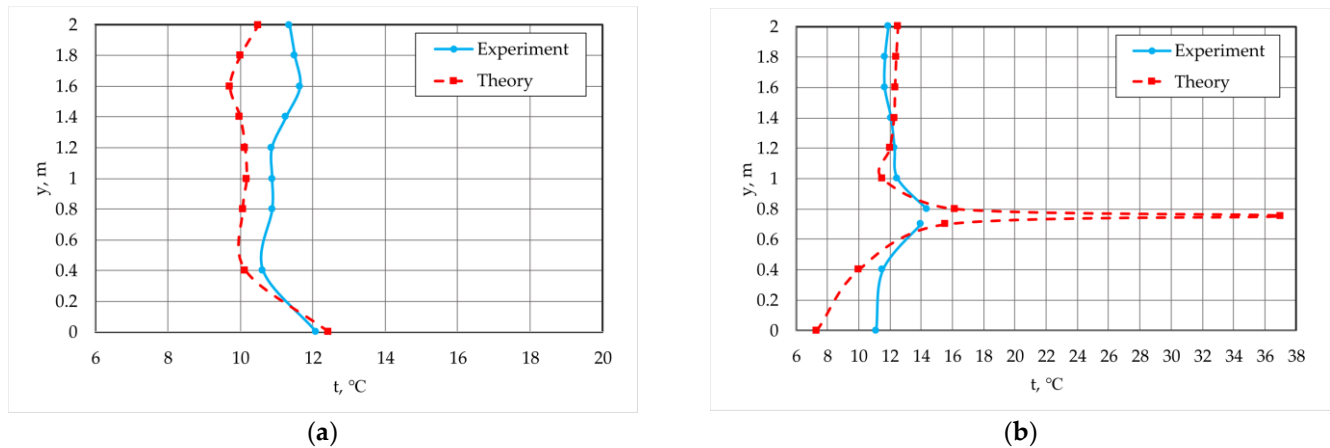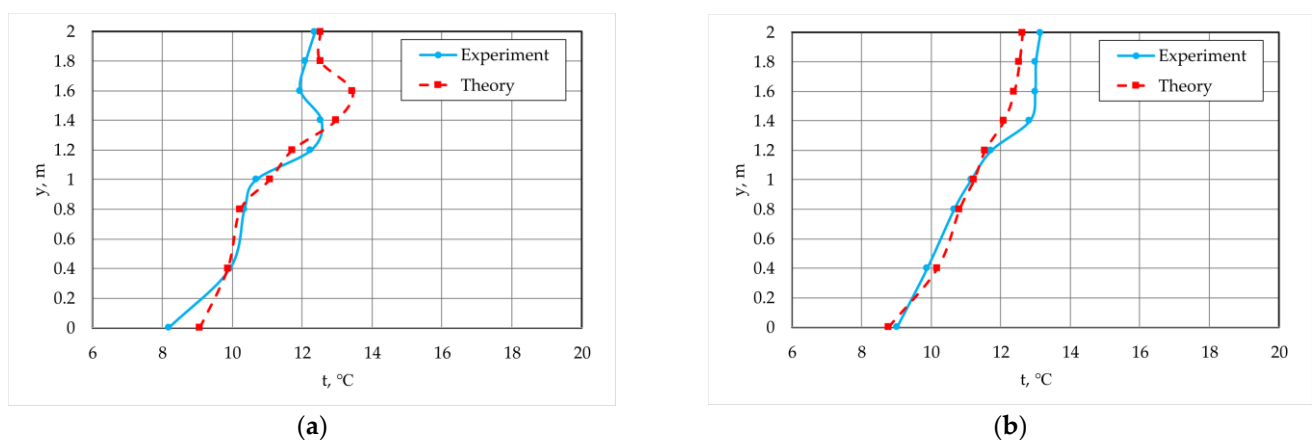**Figure 10.** Distribution of experimental and theoretical values of air temperature along the Y coordinate (τ = 60 min): (**a**) at X = 0.8 m and (**b**) at X = 2.4 m.

It can be noticed that the temperature fields obtained as a result of mathematical modeling and experimental modeling are in good agreement (deviations are no more than 7 % (2 °C)) (Figures 9 and 10). It proves the physical adequacy of the considered adopted heat transfer model. So, it is possible to use this model for analyzing the heat transfer characteristics, taking into account the location of the horizontal panel that simulates the equipment surface.

5. Main Results of Numerical Simulation and Discussion

Figures 11–16 show the main numerical modeling results, illustrating the features of the complex thermo-gravitational flows, hydrodynamics, and the resulting temperature fields in the characteristic sections of the considered area. Different options for the panel location at different heights and at X coordinate relative to the GIH symmetry axis are considered in order to analyze its influence on the premises' thermal conditions (Table 3).

Table 3. Investigation plan for different panel locations in the considered area.

Description of Panel Location	The Coordinates of the Panel Center	Figure Link
The panel is located under the GIH at a height of 0.455 m from the floor	$X_{Tb} = 1.6$ m $Y_{Tb} = 0.455$ m	Figure 11
The panel is located under the GIH at a height of 1.055 m from the floor	$X_{Tb} = 1.6$ m $Y_{Tb} = 1.055$ m	Figure 12
The panel is located near the right wall of the area at a height of 0.755 m from the floor	$X_{Tb} = 0.6$ m $Y_{Tb} = 0.755$ m	Figure 13
The panel is located in the center of the area at a height of 0.755 m from the floor	$X_{Tb} = 2.5$ m $Y_{Tb} = 0.755$ m	Figure 14
The panel is located near the left wall of the area at a height of 0.755 m from the floor	$X_{Tb} = 4.4$ m $Y_{Tb} = 0.755$ m	Figure 15

Figures 11 and 12 show the temperature and velocity fields when the panel is positioned at a distance of 1 m from the left border ($X_{Tb} = 1.6$ m). Figures 11 and 12 correspond to different heights ($Y_{Tb} = 0.455$ m and $Y_{Tb} = 1.055$ m).

Figure 11. Temperature fields (**a**) and streamlines (**b**) for the area with the panel ($X_{Tb} = 1.6$ m, $Y_{Tb} = 0.455$ m) in the GIH operation zone ($\tau = 60$ min).

The numerical results show (Figures 11 and 12) that thermo-gravitational convection forms circulation zones, which are formed by upward currents from surfaces heated by GIH radiation and by downward currents of air cooled due to heat exchange with the relatively cold surfaces of the walls.
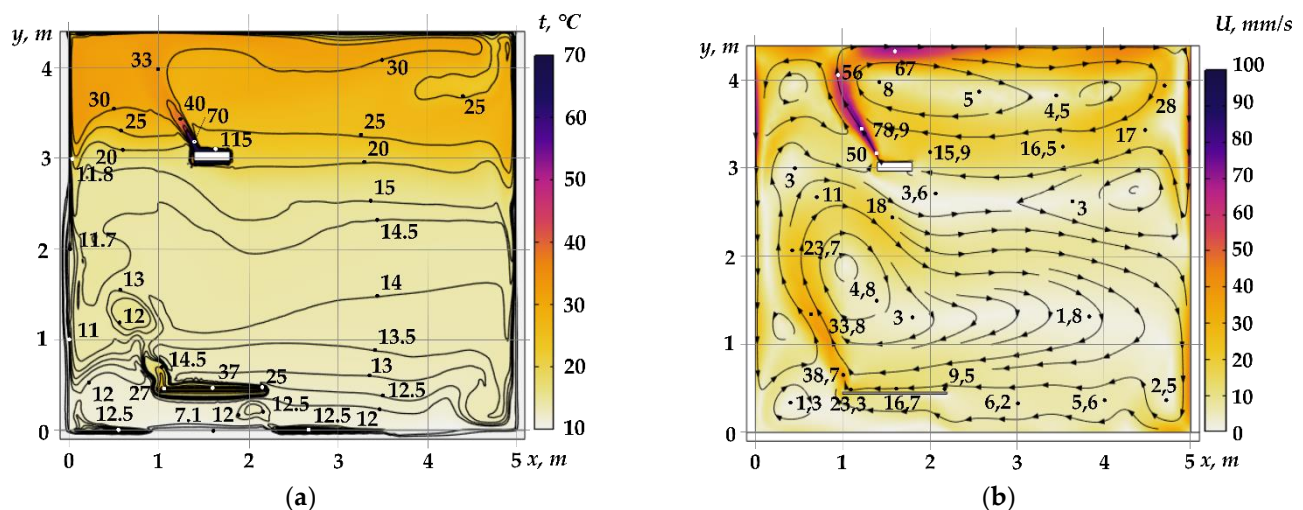
Figure 12. Temperature fields (**a**) and streamlines (**b**) for the area with the panel (X_{Tb} = 1.6 m, Y_{Tb} = 1.055 m) in the GIH operation zone (τ = 60 min).

Lowering the position of the panel (Figures 8, 11 and 12) leads to a displacement of the main ascending flow of heated air to its left side. With an increase in the distance from the floor to the horizontal panel (closer to the GIH), the rise of heated air shifts to the right, while the panel surface warms up more and is already 41 °C on the GIH symmetry axis. In addition, in the case of a panel in a lower position in the study area, the temperatures under the panel are lower than at its higher position. However, on the concrete base to the right and left of the panel (under the conditions of Figure 11), the temperature values are higher than in the second case (Figure 12). It is also noticeable that when the panel is located at a height of Y_{Tb} = 1.055 m (Figure 12), the air above it warms up significantly and at a height of 2 m in the center of the solution area is about 17.5 °C, while at a height of Y_{Tb} = 0.755 m (Figure 11) this value is 14.5 °C. However, at the same time (Figure 12) the temperatures in the lower part on both sides of the panel are lower. It should be noted that the high position of the panel leads to more intensive air masses mixing (Figure 12), higher velocities of circulation currents and the formation of three pronounced circulation zones (from the floor to the horizontal panel $Y < Y_{Tb}$, from the panel to the GIH $Y_{Tb} < Y < Y_{GIH}$ and from GIH to the ceiling $Y > Y_{GIH}$). In the first version (Figure 11), there is no separate zone of air circulation below the panel level, but there is a more extensive zone, covering the lower right part of the study area, in which the temperature values are higher and reach 12.5 °C.

The thermal conditions of the local working area is also indicative of when a panel with a 0.755 m height is located in various areas characteristic of real practice: at the left wall X_{Tb} = 0.6 m (Figure 13); in the center of the premises X_{Tb} = 2.5 m (Figure 14); and at the right wall X_{Tb} = 4.4 m (Figure 15).

It is clearly seen that with identical GIH operation, the panel displacement to the wall causes a radical temperature change in the local working area (Figures 13a, 14a, and 15a) due to an increase in the air movement velocity.

Changing the panel location along the X coordinate located in the zone of GIH influence affects the thermal conditions of the local working zone (Figures 13–15). The most significant heating of the left enclosing structure occurs when the panel is located with coordinates X_{Tb} = 0.6 m, Y_{Tb} = 0.755 m (Figure 13). The thermal plume from the panel surface heated by GIH rises along the wall to 2.5 m from the floor (Figure 13). The numerical values of the wall surface temperatures increase to 13.4 °C (Figure 13), which contributes to additional heat removal through the enclosing structures. In this variant of the panel location in the middle part of the study area from the panel to the GIH $Y_{Tb} < Y < Y_{GIH}$, one significant circulating vortex is formed, covering the entire area of the premises in width. The more heated air, rising along the right wall, then swirls under the heater and, heading towards the right enclosing

structure, descends along it (Figure 13b). It should be noted that the air temperatures in the area between the right wall and the panel also rise to 13.5 °C.
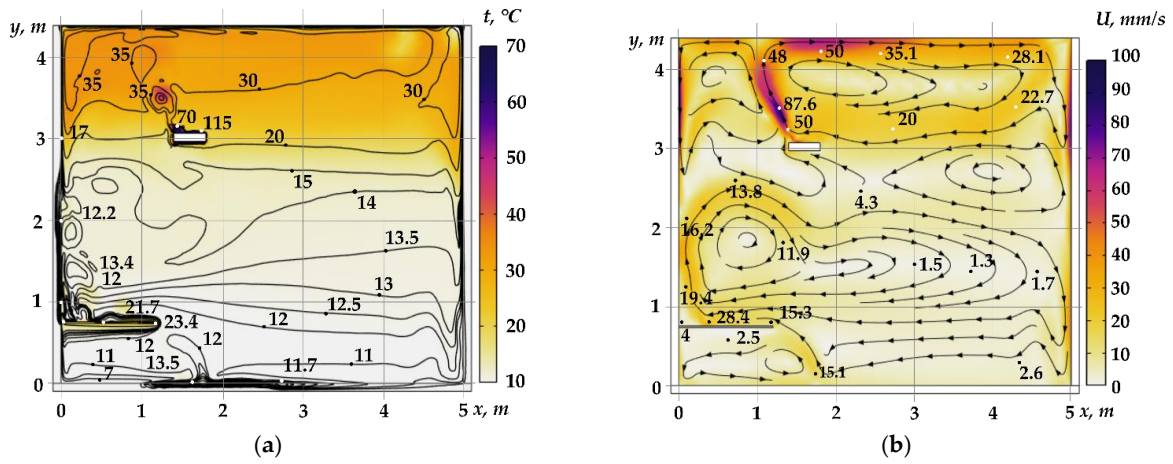

Figure 13. Temperature fields (**a**) and streamlines (**b**) for the area with the panel near the left wall (X_{Tb} = 0.6 m, Y_{Tb} = 0.755 m) at τ = 60 min.
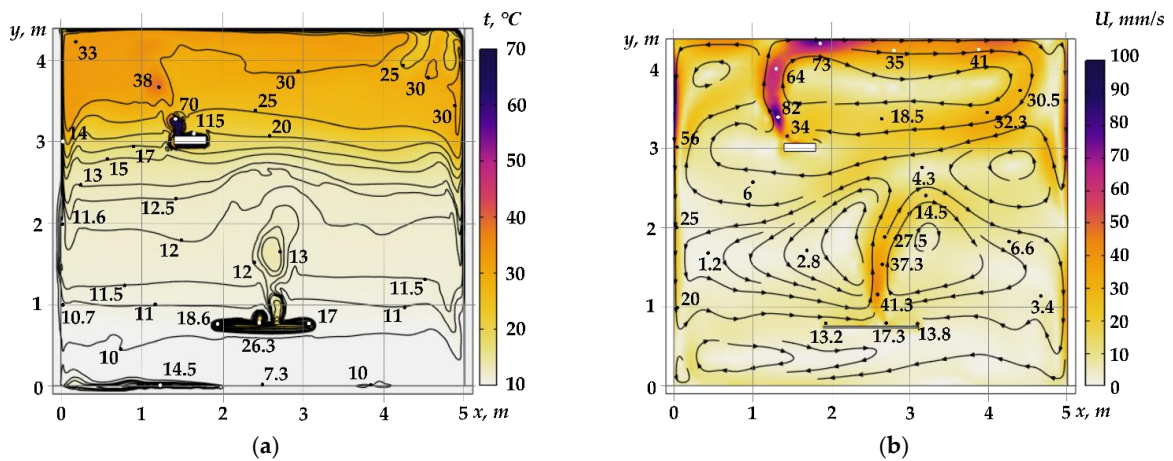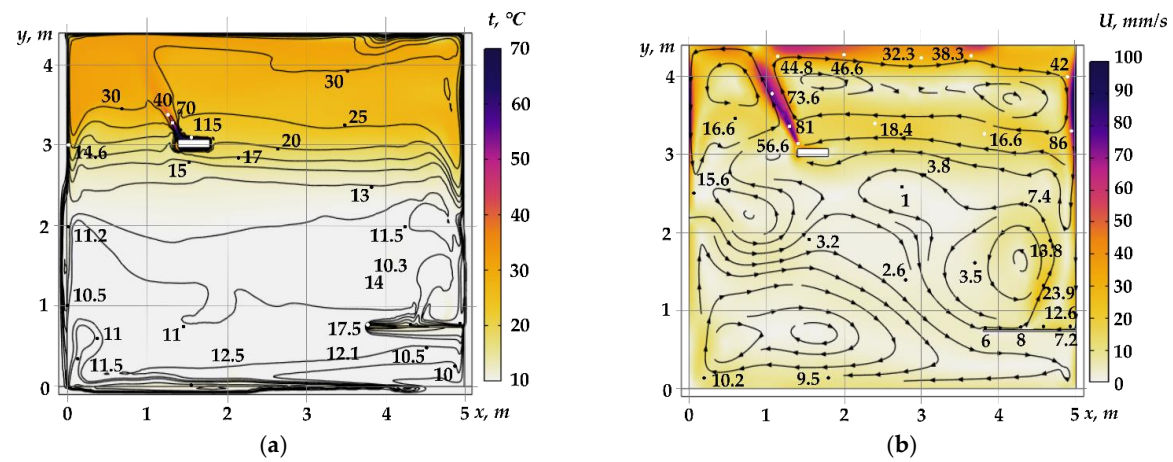

Figure 14. Temperature fields (**a**) and streamlines (**b**) for the area with a panel in the center (X_{Tb} = 2.5 m, Y_{Tb} = 0.755 m) at τ = 60 min.

Figure 15. Temperature fields (**a**) and streamlines (**b**) for the area with a panel near the right wall (X_{Tb} = 4.4 m, Y_{Tb} = 0.755 m) at τ = 60 min.

If the panel is located with coordinates X_{Tb} = 2.5 m, Y_{Tb} = 0.755 m, the rising flow of heated air from the panel is formed almost in the center of this panel (Figure 14a). As

a result, two circulation vortices are formed on both sides of the thermal plume in the case of $Y_{Tb} < Y < Y_{GIH}$ (Figure 14b). Isotherms in the area from the panel to the GIH in this variant are lower (at $Y = 2$ m $T = 12$ °C) than in the previous one (in Figure 13a at $Y = 2$ m $T = 13.5$–14 °C).

Analysis of the results (Figures 8 and 13–15) shows that the least noticeable contribution to the temperature conditions formation is made by the panel location near the right wall (far from the GIH $X_{Tb} = 4.4$ m, $Y_{Tb} = 0.755$ m). Nevertheless, two circulation vortices, formed diagonally relative to each other, are noticeable in Figure 15b. One is above the panel towards the GIH, the other is from the center of the left wall to the lower right corner under the panel. In this case, the air movement speed is relatively small (Figure 15b) and the temperature in the central part at a height of $Y = 2$ m is 11.2 °C.

As for the area from the GIH to the upper enclosing structure $Y > Y_{GIH}$, the changes in the airflow structure and temperature fields are insignificant in all three variants of the panel location along the X coordinate.

Figure 16 shows the results of numerical studies in a characteristic section under the GIH for various options of the panel location relative to the heater. The results for the option when the center of the panel is strictly under the GIH symmetry axis, but at different heights are presented in Figure 16a. The air temperature distribution in the section under the GIH for the variants when the panel is at a standard height $Y_{Tb} = 0.755$ m, but moves along the X coordinate from the left to the right wall.

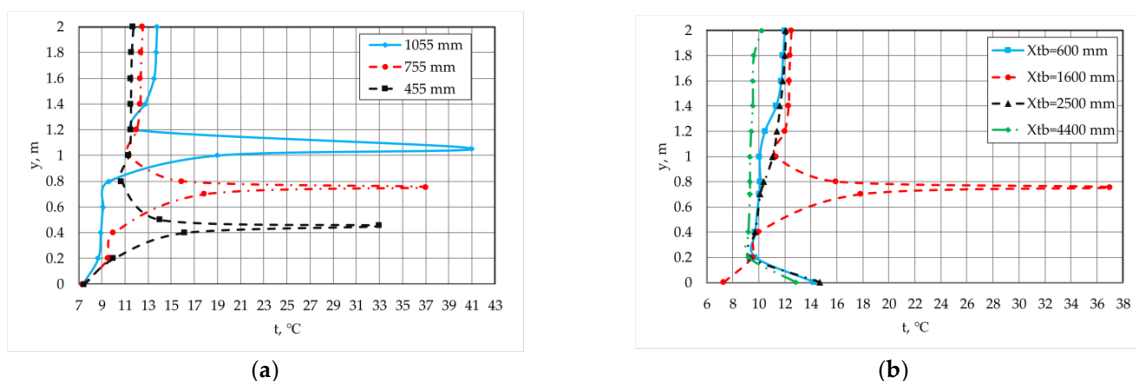(a)   (b)

Figure 16. Air temperature distributions in the section under the GIH at the panel location with coordinates: $X_{Tb} = 1.6$ m and $Y_{Tb} = 0.455$ m; 0.755 m and 1.055 m (a) and at $Y_{Tb} = 0.755$ m and $X_{Tb} = 0.6$ m; 1.6 m; 2.5 m and 4.4 m (b).

Analysis of the results in Figure 16 allows the conclusion to be drawn that moving the panel closer to the GIH (Figures 11 and 12) intensifies the heating of its surface, which leads to stronger air heating and, accordingly, more intense circulating air flows between the panel and the GIH.

When varying the panel location along the X coordinate, there is also a change in the air temperature in the section along the GIH symmetry axis. For three options for installing the panel directly in the zone of the heater influence ($X_{Tb} = 0.6$ m, 1.6 m, and 2.5 m), the air temperatures above it ($Y > 1.0$ m) are practically identical. However, at $X_{Tb} = 1.6$ m, the panel surface itself heats up quite intensely to the temperature of 31.2 °C. Placing the equipment model near the right wall ($X_{Tb} = 4.4$ m) does not significantly affect the temperature distribution over the entire height of the premises. The temperature values are similar to the option when the panel is absent (Figures 5 and 16b).

6. Conclusions

Based on the results of an experimental and theoretical study of heat transfer processes in local working areas of large-sized premises with a heating system based on gas infrared heaters, the possibility of a significant equipment influence on these areas' thermal conditions has been established. Comparison of the results obtained in numerical and

physical modeling shows that the formulated mathematical model can be used to select the thermal conditions of local working areas for any equipment location in the room. It was found that a change in the height of the equipment at any of its positions relative to the symmetry axis of the GIH influence zone leads to a change in the temperature profile in the areas located to the left and right of the equipment (local working areas).

The research results showed that, by changing the position of the equipment relative to the gas infrared heater, it is possible to control the process of formation of not only temperature fields, but also air-mass velocity fields in local working areas. At the same time, it is possible to create both heated to comfortable thermal conditions for the worker, and local areas with a low temperature in the area under study, if it is required.

Author Contributions: Conceptualization, G.V.K.; methodology, V.I.M. and G.V.K.; software, V.I.M. and B.V.B.; validation, B.V.B., V.I.M. and A.V.V.; formal analysis, V.I.M.; investigation, A.V.V. and T.A.N.; writing—original draft preparation, A.V.V.; writing—review and editing, T.A.N.; visualization, A.V.V. and T.A.N.; supervision, G.V.K.; project administration, G.V.K.; funding acquisition, V.I.M. All authors have read and agreed to the published version of the manuscript.

Data Availability Statement: Data available on request due to restrictions of institution.

Nomenclature

GIH	gas infrared heaters
WHR	waste heat recovery
Symbols	
C_p	isobaric heat capacity, [J·kg^{-1}·K^{-1}]
c_μ, $c_{\varepsilon 1}$, $c_{\varepsilon 2}$	parameters in *k-ε* model, [–]
$\vec{g}$	acceleration created by the mass forces, [m/s^2]
F_{Up_GIH}	GIH upper surface area, [m^2]
$\vec{I}$	unit tensor, [–]
k	turbulent kinetic energy, [m^{2}s^{-2}]
Lx	size of the area in the directions *X*, [m]
Ly	size of the area in the directions *Y*, [m]
p	pressure, [Pa]
q_{F_GIE}	determined by rated heat output, [W/m^{-2}]
q_{gas}	conductive-convective heat flux density to this surface, [W/m^{-2}]
q_{rad}	radiation heat density from all radiating surfaces, [W/m^{-2}]
q_{sol}	heat flux density to the surface, [W/m^{-2}]
Q_{V_GIH}	rated heat output, [B$_T$]
T	temperature, [K]
T_{F_GIH}	GIH side surfaces temperature, [K]
$\vec{u}$	velocity vector, [m s^{-1}]
X,Y	coordinates, [m]
Greek symbols	
ε	turbulence dissipation rate, [m^{2}s^{-3}]
η_{Rad}	radiant efficiency [–]
ρ	density, [m^3/kg]
κ	thermal conductivity, [Wm^{-1}K^{-1}]
μ	dynamic viscosity coefficient, [m^{2}s^{-1}]
μ_t	turbulent dynamic viscosity coefficient, [m^{2}s^{-1}]
σ_ε, σ_κ	parameters in *k-ε* model, [–]
τ	time, [s]
Subscripts	
0	initial values
Tb	horizontal panel

References

1. Meha, D.; Dragusha, B.; Thakur, J.; Novosel, T.; Duić, N. A novel spatial based approach for estimation of space heating demand saving potential and CO_2 emissions reduction in urban areas. *Energy* **2021**, *225*, 120251. [CrossRef]
2. Connolly, D.; Lund, H.; Mathiesen, B.V.; Werner, S.; Möller, B.; Persson, U.; Boermans, T.; Trier, D.; Østergaard, P.A.; Nielsen, S. Heat Roadmap Europe: Combining district heating with heat savings to decarbonise the EU energy system. *Energy Policy* **2014**, *65*, 475–489. [CrossRef]
3. Liu, X.; Zhang, T.; Liu, X.; Li, L.; Lin, L.; Jiang, Y. Energy saving potential for space heating in Chinese airport terminals: The impact of air infiltration. *Energy* **2021**, *215*, 119175. [CrossRef]
4. Kobelev, N.; Emelyanov, S.; Kretova, V.; Morzhavin, A.; Amelin, V.; Kobelev, V. Energy-saving Solution in the Heating System of Buildings. *Procedia Eng.* **2015**, *117*, 186–190. [CrossRef]
5. Shen, P.; Wang, Z.; Ji, Y. Exploring potential for residential energy saving in New York using developed lightweight prototypical building models based on survey data in the past decades. *Sustain. Cities Soc.* **2021**, *66*, 102659. [CrossRef]
6. Jezierski, W.; Sadowska, B.; Pawłowski, K. Impact of changes in the required thermal insulation of building envelope on energy demand, heating costs, emissions, and temperature in buildings. *Energies* **2021**, *14*, 56. [CrossRef]
7. *ASHRAE 55-2017*; Standard 55-2017–Thermal Environmental Conditions for Human Occupancy (ANSI/ASHRAE Approved). ASHRAE: Atlanta, GA, USA, 2017.
8. *ISO 7730*; Moderate Thermal Environment–Determination of the PMV and PPD Indices and Specification of the Conditions for Thermal Comfort. International Organization for Standardization: Geneva, Switzerland, 2005.
9. De Dear, R.J.; Brager, G.S. Thermal comfort in naturally ventilated buildings: Revisions to ASHRAE Standard 55. *Energy Build.* **2002**, *34*, 549–561. [CrossRef]
10. Olesen, B.W.; Parsons, K.C. Introduction to thermal comfort standards and to the proposed new version of EN ISO 7730. *Energ. Build.* **2002**, *34*, 537–548. [CrossRef]
11. Li, C.Z.; Zhang, L.; Liang, X.; Xiao, B.; Tam, V.W.Y.; Lai, X.; Chen, Z. Advances in the research of building energy saving. *Energy Build.* **2022**, *254*, 111556. [CrossRef]
12. Yan, C.; Wang, S.; Shan, K.; Lu, Y. A simplified analytical model to evaluate the impact of radiant heat on building cooling load. *Appl. Therm. Eng.* **2015**, *77*, 30–41. [CrossRef]
13. Wang, D.; Wu, C.; Liu, Y.; Chen, P.; Liu, J. Experimental study on the thermal performance of an enhanced-convection overhead radiant floor heating system. *Energy Build.* **2017**, *135*, 233–243. [CrossRef]
14. Yu, T.; Heiselberg, P.; Lei, B.; Pomianowski, M.; Zhang, C.; Jensen, R. Experimental investigation of cooling performance of a novel HVAC system combining natural ventilation with diffuse ceiling inlet and TABS. *Energy Build.* **2015**, *105*, 165–177. [CrossRef]
15. Song, W.; Zhang, Z.; Chen, Z.; Wang, F.; Yang, B. Thermal comfort and energy performance of personal comfort systems (PCS): A systematic review and meta-analysis. *Energy Build.* **2022**, *256*, 111747. [CrossRef]
16. Lin, B.; Wang, Z.; Sun, H.; Zhu, Y.; Ouyang, Q. Evaluation and comparison of thermal comfort of convective and radiant heating terminals in office buildings. *Build. Environ.* **2016**, *106*, 91–102. [CrossRef]
17. Karmann, C.; Schiavon, S.; Bauman, F. Thermal comfort in buildings using radiant vs. all-air systems: A critical literature review. *Build. Environ.* **2017**, *111*, 123–131. [CrossRef]
18. Fallah, M.; Medghalchi, Z. Proposal of a new approach for avoiding Anti-Insulation in residential buildings by considering occupant's comfort condition. *Therm. Sci. Eng. Prog.* **2020**, *20*, 100721. [CrossRef]
19. Sun, H.; Duan, M.; Wu, Y.; Lin, B.; Yang, Z.; Zhao, H. Thermal performance investigation of a novel heating terminal integrated with flat heat pipe and heat transfer enhancement. *Energy* **2021**, *236*, 121411. [CrossRef]
20. Oravec, J.; Šikula, O.; Krajčík, M.; Arıcı, M.; Mohapl, M. A comparative study on the applicability of six radiant floor, wall, and ceiling heating systems based on thermal performance analysis. *J. Build. Eng.* **2021**, *36*, 102133. [CrossRef]
21. Jiang, S.; Li, X.; Lyu, W.; Wang, B.; Shi, W. Numerical investigation of the energy efficiency of a serial pipe-embedded external wall system considering water temperature changes in the pipeline. *J. Build. Eng.* **2020**, *31*, 101435. [CrossRef]
22. Zhang, C.; Pomianowski, M.; Heiselberg, P.K.; Yu, T. A review of integrated radiant heating/cooling with ventilation systems-Thermal comfort and indoor air quality. *Energy Build.* **2020**, *223*, 110094. [CrossRef]
23. Peng, P.; Gong, G.; Deng, X.; Liang, C.; Li, W. Field study and numerical investigation on heating performance of air carrying energy radiant air-conditioning system in an office. *Energy Build.* **2020**, *209*, 109712. [CrossRef]
24. Võsa, K.-V.; Ferrantelli, A.; Kurnitskia, J. A combined analytical model for increasing the accuracy of heat emission predictions in rooms heated by radiators. *J. Build. Eng.* **2019**, *23*, 291–300. [CrossRef]
25. Cardemil, J.M.; Schneider, W.; Behzad, M.; Starke, A.R. Thermal analysis of a water source heat pump for space heating using an outdoor pool as a heat source. *J. Build. Eng.* **2019**, *3*, 101581. [CrossRef]
26. Gourlis, G.; Kovacic, I. Building Information Modelling for analysis of energy efficient industrial buildings–A case study. *Renew. Sustain. Energy Rev.* **2017**, *68*, 953–963. [CrossRef]
27. Meng, X.; Wang, Y.; Liu, T.; Xing, X.; Cao, Y.; Zhao, J. Influence of radiation on predictive accuracy in numerical simulations of the thermal environment in industrial buildings with buoyancy-driven natural ventilation. *Appl. Therm. Eng.* **2016**, *96*, 473–480. [CrossRef]
28. Ascione, F.; Bianco, N.; Iovane, T.; Mauro, G.M.; Napolitano, D.F.; Ruggiano, A.; Viscido, L. A real industrial building: Modeling, calibration and Pareto optimization of energy retrofit. *J. Build. Eng.* **2020**, *29*, 101186. [CrossRef]

29.　De Angelisa, A.; Saro, O.; Truant, M. Evaporative cooling systems to improve internal comfort in industrial buildings. *Energy Procedia* **2017**, *126*, 313–320. [CrossRef]

30.　Liu, G.; Zhou, X.; Yan, J.; Yan, G. A temperature and time-sharing dynamic control approach for space heating of buildings in district heating system. *Energy* **2021**, *221*, 119835. [CrossRef]

31.　Moutinho, V.; Moreira, A.C.; Silva, P.M. The driving forces of change in energy-related CO_2 emissions in Eastern, Western, Northern and Southern Europe: The LMDI approach to decomposition analysis. *Renew. Sustain. Energy Rev.* **2015**, *50*, 1485–1499. [CrossRef]

32.　Yang, L.; Yan, H.; Lam, J.C. Thermal comfort and building energy consumption implications–A review. *Appl. Energy* **2014**, *115*, 164–173. [CrossRef]

33.　Kurilenko, N.I.; Kurilenko, E.Y.; Mamontov, G.Y. New approach to microclimate parameter selection for the production area with heat supply systems based on gas infrared radiators. *EPJ Web Conf.* **2016**, *110*, 01033. [CrossRef]

34.　Kuznetsov, G.V.; Kurilenko, N.I.; Maksimov, V.I.; Nagornova, T.A. Experimental and numerical study of heat transfer in production area heated by gas infrared source. *Int. J. Therm. Sci.* **2020**, *154*, 106396. [CrossRef]

35.　Kuznetsov, G.V.; Maksimov, V.I.; Nagornova, T.A. Prognostic potential of free convection models for analysis of thermal conditions of heat supply objects. *Therm. Sci.* **2018**, *22*, 545–556. [CrossRef]

36.　Wang, H.; Xu, M.; Bian, C. Experimental comparison of local direct heating to improve thermal comfort of workers. *Build. Environ.* **2020**, *177*, 106884. [CrossRef]

37.　Rhee, K.-N.; Kim, K.W. A 50 year review of basic and applied research in radiant heating and cooling systems for the built environment. *Build. Environ.* **2015**, *91*, 166–190. [CrossRef]

38.　Lee, E.H. 2.30 A Review on Applications of Infrared Heating for Food Processing in Comparison to Other Industries. In *Innovative Food Processing Technologies*; Knoerzer, K., Muthukumarappan, K., Eds.; Elsevier: Amsterdam, The Netherlands, 2021; pp. 431–455. [CrossRef]

39.　Wang, H.; Kaur, S.; Elzouka, M.; Prasher, R. A nano-photonic filter for near infrared radiative heater. *Appl. Therm. Eng.* **2019**, *153*, 221–224. [CrossRef]

40.　Maznoy, A.; Kirdyashkin, A.; Pichugin, N.; Zambalov, S.; Petrov, D. Development of a new infrared heater based on an annular cylindrical radiant burner for direct heating applications. *Energy* **2020**, *204*, 117965. [CrossRef]

41.　Lee, E.-H.; Yang, D.-Y. Experimental and numerical analysis of a parabolic reflector with a radiant heat source. *Int. J. Heat Mass Transf.* **2015**, *85*, 860–864. [CrossRef]

42.　Brown, K.J.; Farrelly, R.; O'Shaughnessy, S.M.; Robinson, A.J. Energy efficiency of electrical infrared heating elements. *Appl. Energy* **2016**, *162*, 581–588. [CrossRef]

43.　Kavga, A.; Karanastasi, E.; Konstas, I.; Panidis, T. Performance of an Infrared Heating System in a Production Greenhouse. *IFAC Proc.* **2013**, *46*, 235–240. [CrossRef]

44.　Maksimov, V.I.; Nagornova, T.A.; Kurilenko, N.I.; Voloshko, I.V. Advantage analysis of systems for ensuring local working zones thermal conditions based on gas infrared emitters in comparison with traditional convective heating systems. *Bull. Tomsk. Polytech. Univ. Geo Assets Eng.* **2021**, *332*, 128–141. [CrossRef]

45.　Dudkiewicz, E.; Szałański, P. Overview of exhaust gas heat recovery technologies for radiant heating systems in large halls. *Therm. Sci. Eng. Prog.* **2020**, *18*, 100522. [CrossRef]

46.　Dudkiewicz, E.; Jeżowiecki, J. The influence of orientation of a gas-fired direct radiant heater on radiant temperature distribution at a work station. *Energy Build.* **2011**, *43*, 1222–1230. [CrossRef]

47.　Kuznetsov, G.V.; Kurilenko, N.I.; Maksimov, V.I.; Mamontov, G.Y.; Nagornova, T.A. Heat transfer under heating of a local region of a large production area by gas infrared radiators. *J. Eng. Phys. Thermophys.* **2013**, *86*, 519–524. [CrossRef]

48.　Mikhailenko, S.A.; Miroshnichenko, I.V.; Sheremet, M.A. Thermal radiation and natural convection in a large-scale enclosure heated from below: Building application. *Build. Simul.* **2021**, *14*, 681–691. [CrossRef]

49.　Kurilenko, N.I.; Mamontov, G.Y.; Mikhaylova, L.Y. Temperature patterns in the gas infrared radiator heating area. *EPJ Web Conf.* **2015**, *82*, 01006. [CrossRef]

50.　Kuznetsov, G.V.; Maksimov, V.I.; Nagornova, T.A.; Voloshko, I.V.; Gutareva, N.Y.; Kurilenko, N.I. Experimental determination of the worker's clothing surface temperature during the ceramic gas heater operation. *Therm. Sci. Eng. Prog.* **2021**, *22*, 100851. [CrossRef]

51.　U.S. Department of Energy. DOE Fundamentals handbook. In *Thermodynamics, Heat Transfer and Fluid Flow (Volume 2 of 3)*; U.S. Department of Energy: Washington, DC, USA, 2016.

52.　Haynes, W.M. *Handbook of Chemistry and Physics 2015–2016*; CRC/Taylor & Francis: Boca Raton, FL, USA, 2015.

53.　Hesaraki, A.; Huda, N. A comparative review on the application of radiant low-temperature heating and high-temperature cooling for energy, thermal comfort, indoor air quality, design and control. *Sustain. Energy Technol. Assess.* **2022**, *49*, 101661. [CrossRef]

54.　Batchelor, G.K. *An Introduction to Fluid Dynamics*; Cambridge University Press: Cambridge, UK, 2000.

55.　Tritton, D.J. *Physical Fluid Dynamics*, 2nd ed.; Clarendon Press: Oxford, UK, 1988.

56.　Wilcox, D.C. *Turbulence Modeling for CFD*, 2nd ed.; DCW Industries: Mumbai, India, 1988.

57. Kuzmin, D.; Mierka, O.; Turek, S. On the Implementation of the k-ε Turbulence Model in Incompressible Flow Solvers Based on a Finite Element Discretization. *Int. J. Comput. Sci. Math.* **2007**, *1*, 193–206. [CrossRef]
58. Siegel, R.; Howell, J. *Thermal Radiation Heat Transfer*, 4th ed.; Taylor & Francis: New York, NY, USA, 2002.